Transient pool boiling in microgravity†

J. S. ERVIN,‡ H. MERTE, JR.,§ R. B. KELLER§ and K. KIRK§

‡ Mechanical and Aerospace Engineering Department, University of Dayton, Dayton, OH, U.S.A.
§ Department of Mechanical Engineering and Applied Mechanics, University of Michigan, Ann Arbor, MI, U.S.A.

Abstract—Transient nucleate pool boiling experiments using R113 are conducted for short times in microgravity and in earth gravity with different heater surface orientations and subcoolings. The heating surface is a transparent gold film sputtered on a quartz substrate, which simultaneously provides surface temperature measurements and permits viewing of the boiling process from beneath. For the microgravity experiments, which have uniform initial temperatures and no fluid motion, the temperature distribution in the R113 at the moment of boiling inception is known. High speed cameras with views both across and through the heating surface record the boiling spread across the heater surface, which are classified into six (6) distinct categories.

INTRODUCTION

THIS PAPER presents initial results of experiments in which the influence of known liquid temperature distributions on nucleation and the subsequent phase change dynamics in transient nucleate pool boiling are examined. In the absence of buoyancy, an initially motionless liquid remains stagnant upon heating until the onset of boiling, and the temperature distribution at the moment of incipient boiling can be determined from a conduction heat transfer analysis. The period of microgravity is short at the present time, limited to 5.1 s by the height of the drop tower used, but extended times are planned for the future. A step change in heat flux is imposed in microgravity, where the quiescent fluid has an initial uniform temperature for various subcooling levels, and the pressure of the system is maintained constant.

Liquid motion, whether induced by buoyancy or externally forced, influences the liquid temperature distribution near the heater surface, and, for a given heat flux, results in temperature levels below that with a stagnant liquid. The heater surface temperature at incipient boiling and the ensuing bubble dynamics may be surmised to be different for the two temperature distributions arising from the presence or absence of liquid motion. For transient pool boiling in earth gravity where the liquid is initially motionless, buoyancy will quickly initiate bulk liquid motion during the heating of the liquid. Studies of the onset of natural convection occurring before boiling inception in a heated liquid pool at earth gravity or greater effective body forces are reviewed in Ulucakli [1]. Additional works concerning the transient heating of a liquid pool in earth gravity include that of Oker and

Merte [2] and Ngheim [3]. In ref. [4], it was shown that incipient boiling resulting from transient heating of flat surfaces occurred at a considerably larger surface temperature for the horizontal up orientation in earth gravity than with microgravity, with all other test conditions held constant.

Straub et al. [5] summarized the results of the German microgravity boiling experimental program beginning in the mid-1970s, which made use of sounding rockets and parabolic aircraft flights. They concluded that the effect of buoyancy on nucleate pool boiling is small. Many of the tests used heated wires, where the diameters of these wires were comparable to or smaller than the size of the vapor bubbles nucleating on them. Surface tension effects on vapor bubble motion are quite different for wires as compared to flat surfaces, and the wires were sometimes completely enveloped by vapor at boiling inception, with subsequent surface tension effects producing a 'pseudo' film boiling. The flat heater surface used in the present study was large relative to the early bubble sizes, and permitted the clear observation of quite distinct categories of bubble dynamics resulting from changes in buoyancy from earth gravity to microgravity.

EXPERIMENTAL APPARATUS

Transient pool boiling experiments were conducted in both earth gravity and short term microgravity. The pool boiling experiments in the laboratory were conducted with heater surface orientations of $a/g = \pm 1$ relative to the gravity vector, achieved by inverting the test vessel from horizontal up for $a/g = +1$ to horizontal down for $a/g = -1$. The microgravity experiments were performed in the evacuated 132 m drop tower at the NASA Lewis Research Center, which provided 5.18 s of free fall with effective body forces on the order of 10^{-5} g. The heat flux,

NOMENCLATURE

a	acceleration [m s^{-2}]; thermal diffusivity		δ^*	superheated thermal boundary layer
c	specific heat [kJ kg^{-1} K^{-1}]			thickness [mm]
g	gravitational acceleration [m s^{-2}]		Δ	change.
k	thermal conductivity			
q''	heat flux [W cm^{-2}]			
R	electrical resistance [Ω]		Subscripts	
T	temperature [°C]		i	initial
t	time [s]		hom	homogeneous nucleation
U	internal energy [kJ]		l	liquid
x	x coordinate.		s	saturation
			sub	subcooling
Greek symbols			T	total
δ	thermal boundary layer thickness [mm]		w	heater surface.

heater surface temperature, pressure near the heating surface, and liquid bulk temperature were measured in each of the independent test vessels used. High speed video recordings of the earth gravity experiments and high speed black and white movies for the microgravity tests were made with two orthogonal views, across and through each test surface.

The drop vessel and associated electronics were designed to withstand the vacuum conditions and the 50 g impact at the bottom of the drop tower. The drop vessel shown in Fig. 1 contained two heater test surfaces, located on the bottom surface, and consisted of thick aluminum plates to provide uniform temperature conditions at the start of a test, while film heaters mounted externally established the initial temperature level of the test fluid. Fins welded to the inner walls of the vessel increased the heat transfer to the test fluid for improved temperature uniformity, with resulting stratifications of less than 0.2°C.

The laboratory vessel was also fabricated of aluminum with the same internal configuration as the drop vessel, but was double-walled so that a thermostatically controlled circulating water-ethylene glycol mixture maintained a temperature uniformity to within 0.06–0.11°C (0.11–0.20°F) at an operating level of 49°C. Trunnions permitted rotation between the heater facing horizontal up and horizontal down with respect to earth gravity.

The heating surface is a 400 Å thick semi-transparent gold film sputtered on a quartz substrate, highly polished with 1.4 micron pitch polish, and serves simultaneously as a heater and a resistance thermometer. The heater is rectangular in shape, 1.91 cm by 3.81 cm (0.75 inches by 1.5 inches), as shown in Fig. 2, and was intended to be considerably larger than the size of the bubbles expected to be formed on it. The current conducting and voltage measuring leads consisted of gold films 10 000 Å thick.
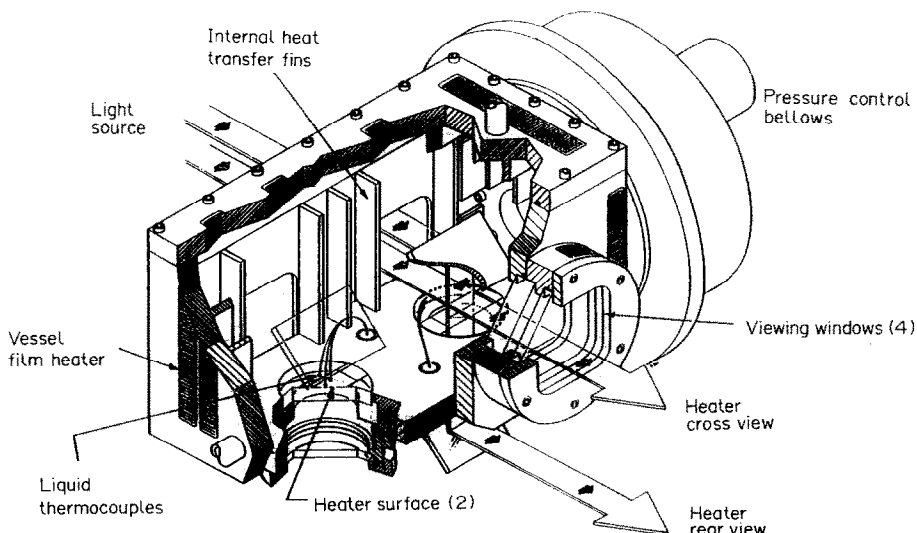

FIG. 1. Drop test vessel.

Gold Film Surface

PARTS
1 Teflon Support Ring
2 Quartz
3 Current Leads 1000 Å
  Gold Layer
4 Semi-Transparent
  Gold Boiling Surface 1.5" X
  0.75" X ≈400 Å
5 Potential Leads
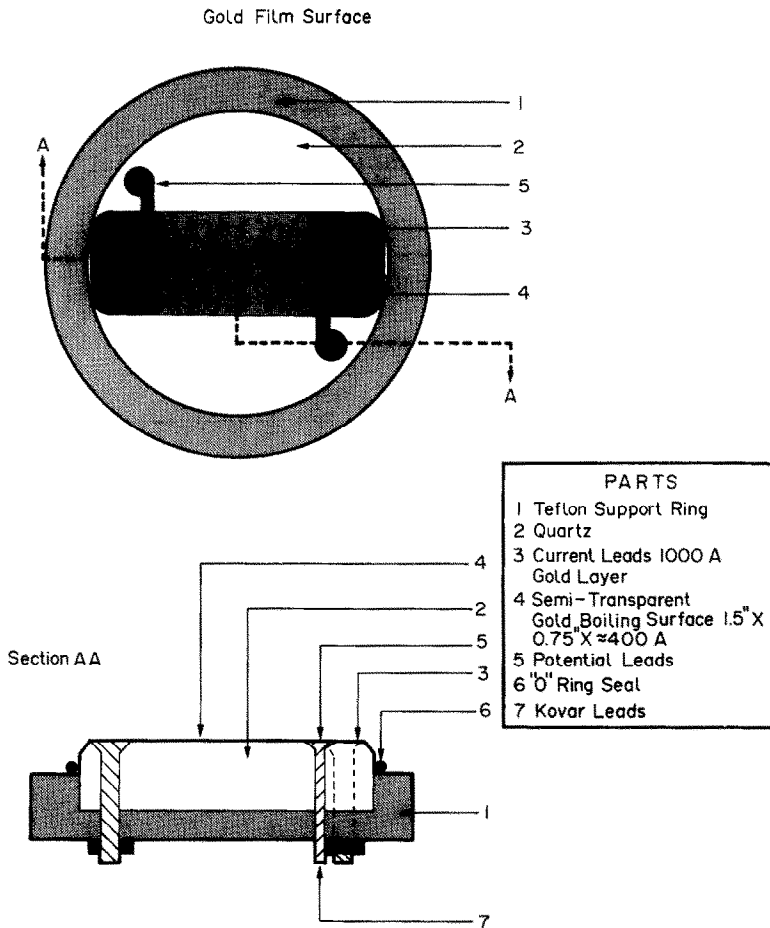6 'O' Ring Seal
7 Kovar Leads

Section AA

FIG. 2. Gold film heater surface.

As in the work of Oker and Merte [4], it was found that the electrical resistance of the gold surfaces varied with time, but that the slope of the linear relationship of surface resistance and temperature, dR/dT, remained essentially constant for each particular surface. This resistance change was attributed to an aging effect, and was initially accelerated by tempering at a temperature of about 275°C for 20 min, following which the temperature–electrical resistance relation for each surface was determined by calibration. The thin film heater resistance was calibrated in place prior to each test at the ambient temperature, in order to correct for the slow drift of the calibration, and is referred to as the single point calibration.

The power supply provided a constant voltage across the thin film surface for the boiling tests with a step increase in power input. Since the resistance of the thin film test surfaces during heating changed in the order of just a few percent, the heat flux was maintained essentially constant. The power supply could accept either a microprocessor input or a manual voltage pot signal as an input, and provided an output signal to the base of the power transistors, which in turn powered the thin film surface heater.

Calibrated shunts were used for the determination of the current.

Commercial grade R113 (trichlorotrifluoroethane, CCl_2FCClF_2) was used for all of the experiments. This fluid was chosen because: (1) its properties are well established and representative of 'space fluids' such as cryogens and other fluorocarbons, (2) the low normal boiling point (47.6°C) minimized problems associated with heat loss to the surroundings, and (3) it is electrically non-conductive, which made it compatible for direct contact with the thin gold film heater.

A special degassing procedure was necessary, involving a combination of distillation at room temperature, leaving behind the high boiling point components such as oils and solids, and freezing on fins with liquid nitrogen under low pressure, so that air components, except for water vapor and CO_2, were eliminated. A molecular sieve with a four angstrom effective pore size served as a mechanical filter and to remove the water vapor and CO_2.

The fluid pressure was maintained constant with an active control system. A seven inch diameter stainless steel bellows isolated the test fluid from the gas used

First surface mirrors
M2, M3, M5

Reflecting prism, 45°
PI

Light sources
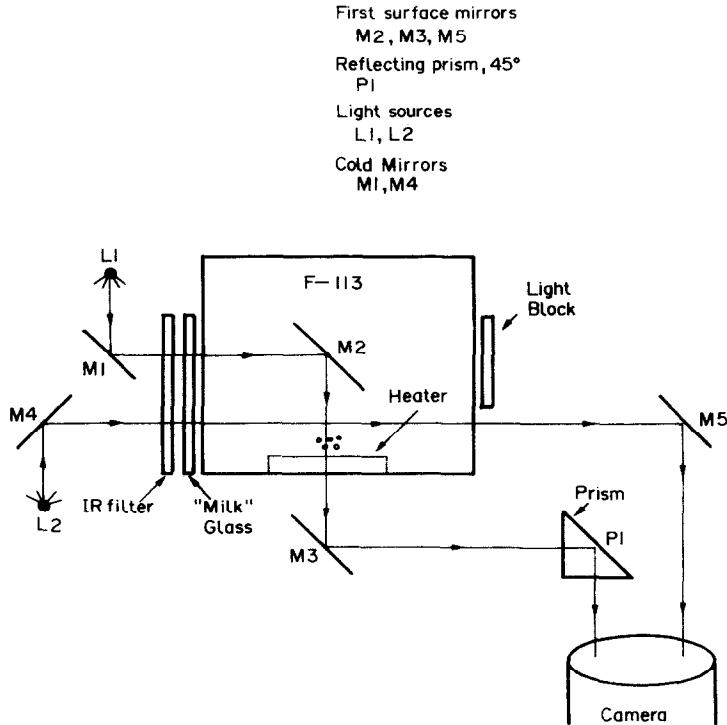LI, L2

Cold Mirrors
MI, M4

FIG. 3. Schematic of optical system for two orthogonal views.

to regulate the pressure. Solenoid valves and a proportional valve were controlled by appropriate electronic circuits. The pressure level was controlled to within ±0.172 kPa (±0.025 psi) of the set point pressure, corresponding to ±0.06°C (±0.1°F) of the saturation temperature for R113, except for a very short period on the order of several milliseconds immediately following nucleation. The desired subcooling was obtained by increasing the system pressure above the saturation pressure corresponding to the initial liquid temperature.

A microprocessor controlled data acquisition system was used to measure voltages from the thermocouples, the pressure transducer, and the heater surface, in addition to sequencing the various events associated with the drop test. This unit had the capability of recording data at eight voltage ranges from ±1.5 mV (with a resolution of 50 nanovolts) to ±5 V (with a resolution of 166 microvolts).

Chromel-constantan Teflon sheathed thermocouples with ungrounded junctions were used for the measurement of the R113 temperature. The reference junctions were maintained in a stainless steel dewar containing crushed ice and water, sealed from the external vacuum of the drop tower. The final accuracy of the temperature measurement as determined by calibration was on the order of ±0.05°C.

Two views of the heating surface were recorded in all experiments for purposes of determining the incipient boiling time and for observation of the phase change dynamics. The optical arrangement used is shown in Fig. 3. Different imaging cameras were used for the laboratory pool boiling vessel and the drop vessel; a Kodak Ektapro 1000 Image System operated at speeds up to 1000 frames per second, and a D. B. Milliken high speed camera at 400 pictures per second, respectively. Each camera was synchronized with the powering of the heater surface to establish a time reference with the data acquisition system.

Further details of the experimental apparatus are given in Ervin [6].

EXPERIMENTAL PROCEDURE

Following the single point calibration, the test vessel was heated to a steady-state uniform R113 temperature distribution within the vessel, indicated by the internal thermocouples. A cool-down period of 45 min for the heater surface between laboratory tests provided the same reproducibility of the boiling inception surface temperature (within 5% of the previous value) as that obtained by waiting 36 h and permitted the observable vapor bubbles to collapse.

Three tests were performed sequentially in connection with each drop experiment: a pre-drop test with high speed photography, a drop test with high speed photography, and a post drop test with no photography. The pre-drop test was identical to the drop test but was conducted at earth gravity and served as a reference for comparison to the microgravity test. After the test package was dropped and

retrieved from the bottom of the drop tower, the post drop test was then performed to verify the proper operation condition of the circuitry and mechanical hardware.

The actual drop test procedure will now be described in some detail. Data acquisition and control instructions were transferred from a portable computer to the data acquisition system mounted on the drop bus. The software provided instructions for measuring the bulk liquid temperature, and then set the specified subcooling level, based on this measured bulk liquid temperature, by adjusting the pressure level inside the vessel through actuation of the bellows pressure control system. The voltage level to be applied to the heater surface to produce the desired heat flux was also set. The protective outer skins were installed on the drop bus, and the bus placed into position at the top of the drop tower, at which time evacuation began. At the desired vacuum level and R113 temperature the camera lights and the high speed camera were energized, followed by the release of the drop bus in the drop tower. At the onset of the free fall, the heater was powered and the data acquisition initiated.

The independent variables in the tests were : surface type, different quartz surfaces ; bulk liquid subcooling, nominally 0, 3, or 11°C ; and total heat flux, nominal levels of 4, 6, and 8 W cm^{-2}. A heat flux level of 2 W cm^{-2} was used in the laboratory pool boiling experiments but not in the drop experiments, because it was observed that even at a power input of 4 W cm^{-2} the time required for the onset of boiling in microgravity was greater than the five second microgravity period available in the drop tower. The dependent test variables were the voltages across the heater surface and shunt, and the pressure transducer voltage, which provided the mean instantaneous heater surface temperature, heat flux, and system pressure, respectively. At times, a liquid temperature measurement near and over the heater surface was also included.

Data reduction

The spatial mean gold film heater surface temperature is determined from the measured test surface resistance, the single point calibration resistance, with its corresponding known temperature, and the slope of the calibration curve. The heater surface temperatures were determined with an uncertainty of ±1.0°C.

The heat transfer to the liquid, q_l'', could be calculated by a transient one-dimensional conduction analysis with the measured total heat flux, q_T'', under circumstances which permitted reasonable analytical assumptions. Assuming one-dimensional conduction in a semi-infinite media with a constant plane heat source, the ratio of the heat flux transferred to the liquid and to the quartz is a constant

$$\frac{q_l''}{q_T''} = 0.175 \qquad (1)$$

for the combination of R113 and quartz. With the measurement of q_T'', the heat flux to the test fluid is thus known, and also permitted the comparison between the measured and computed surface temperatures. The maximum uncertainty in the total power input per unit area, q_T'', was ±0.18 W cm^{-2}, and the total uncertainty in q_l'' calculated from equation (1) is ±4%.

RESULTS

Figure 4 presents the one-dimensional conduction prediction for a semi-infinite media with an imposed heat flux

$$\Delta T_i = T(x) - T_i = \frac{2q_l''}{k_1}\sqrt{\left(\frac{\alpha t}{\pi}\right)}\exp\left(\frac{-x^2}{4\alpha t}\right)$$
$$- \frac{q_l''x}{k_1}\text{erfc}\left(\frac{x}{2\sqrt{(\alpha t)}}\right). \qquad (2)$$

Included are the measured transient heater surface temperatures in earth gravity for both the horizontal up and horizontal down orientations and in microgravity, with otherwise similar conditions. For Run 79 the heater surface faces horizontal up in earth gravity, and the onset of natural convection appears as an irregularity in the temperature–time plot. This irregularity coincides with the observed onset of fluid motion and the departure of the heater surface temperature from the one-dimensional semi-infinite media conduction prediction.

Following the onset of natural convection, incipient boiling occurred, as indicated. Incipient boiling occurred in some tests when the mean heater surface temperature reached a maximum, while in other cases the onset of boiling occurred prior to this point. For cases in which the latter occurred, the level of the ensuing maximum heater surface temperature depended on the manner in which the boiling propagated across the heated surface. If incipient boiling occurred as an almost explosive event over the entire heater surface, then the temperature associated with boiling incipience was the maximum surface temperature. If boiling inception occurred at a heater corner, for example, the heater would be cooled locally while the remainder of the heater surface continued to rise in temperature. Since the heater surface temperature measured is spatially averaged, the measured temperature would continue to rise until boiling propagated sufficiently to produce a subsequent decrease in the mean value. A quasi-steady boiling region is noted in Fig. 4 for Run 79. In this domain of the temperature–time plot, boiling has spread across the entire heating surface, and the quasi-steady boiling temperature level is less than the maximum heater surface temperature but above the saturation temperature for the liquid at the system pressure.
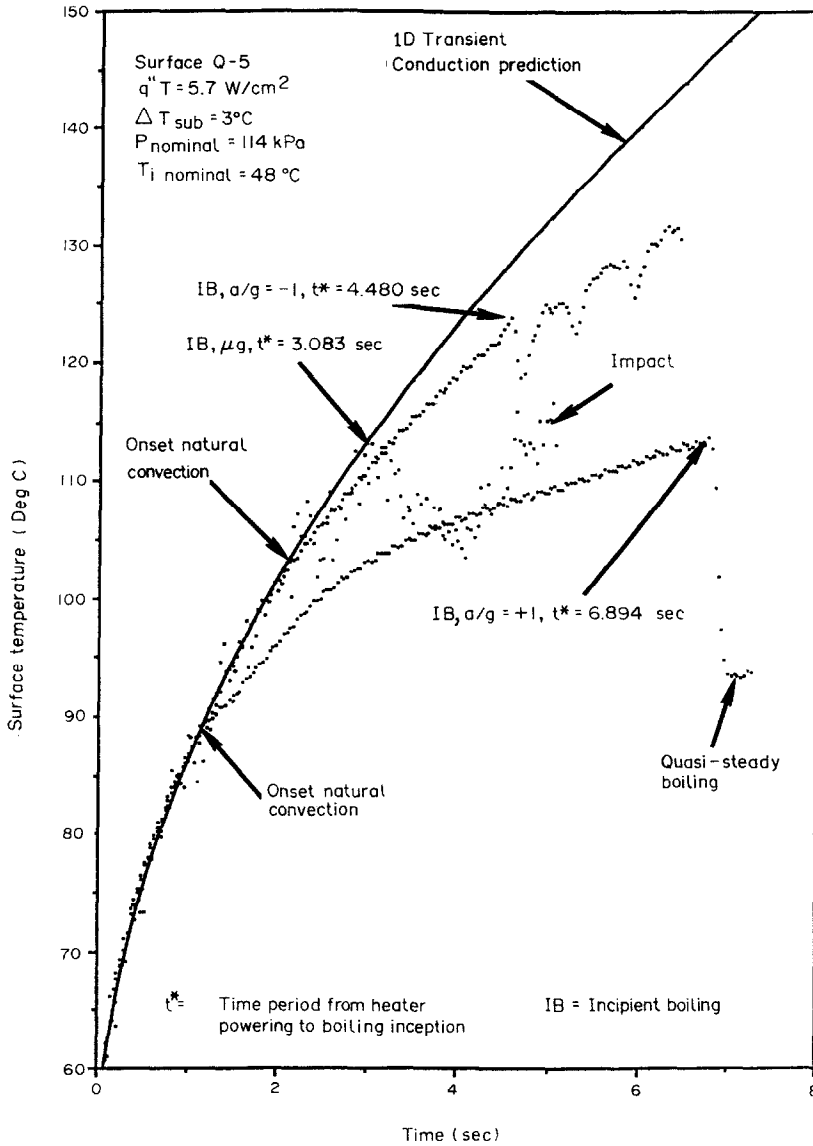
FIG. 4. Measured transient heater surface temperatures for $a/g = \pm 1$ and microgravity with otherwise similar conditions.

The heater surface temperature–time plot for Run 75 in Fig. 4 is for experimental conditions identical to those of Run 79, except that the heater surface is now inverted in earth gravity. The departure from the one-dimensional conduction prediction indicates the onset of natural convection, and the incipient boiling point subsequently appears as a disturbance. The onset of boiling and its spread across the heated surface causes a drop in the measured surface temperature. Once the boiling has spread over the entire heating surface, buoyancy holds the vapor at the heating surface and, as a consequence, the temperature of the heater surface rises. Periodicities superimposed on the mean surface temperature are observed because the vapor alternately collapses and grows near the edges of the heater.

The spatial mean temperature–time plot for a microgravity experiment is also presented in Fig. 4. The measured temperature follows the one-dimensional conduction solution until incipient boiling occurs. At the level of microgravity present in these tests, there was no liquid motion resulting from the heating of the liquid. Following the onset of boiling, a single large vapor bubble covered the heater surface, effectively insulating it from the liquid. Some increased scatter observed in this test was due to noise, since eliminated. This was the only microgravity test whose initial conditions coincided with those at $a/g = \pm 1$.

The measured heater surface temperatures provide data with which the calculated liquid temperatures at the surface are later compared. In addition, thermocouple measurements confirm the basis for one-
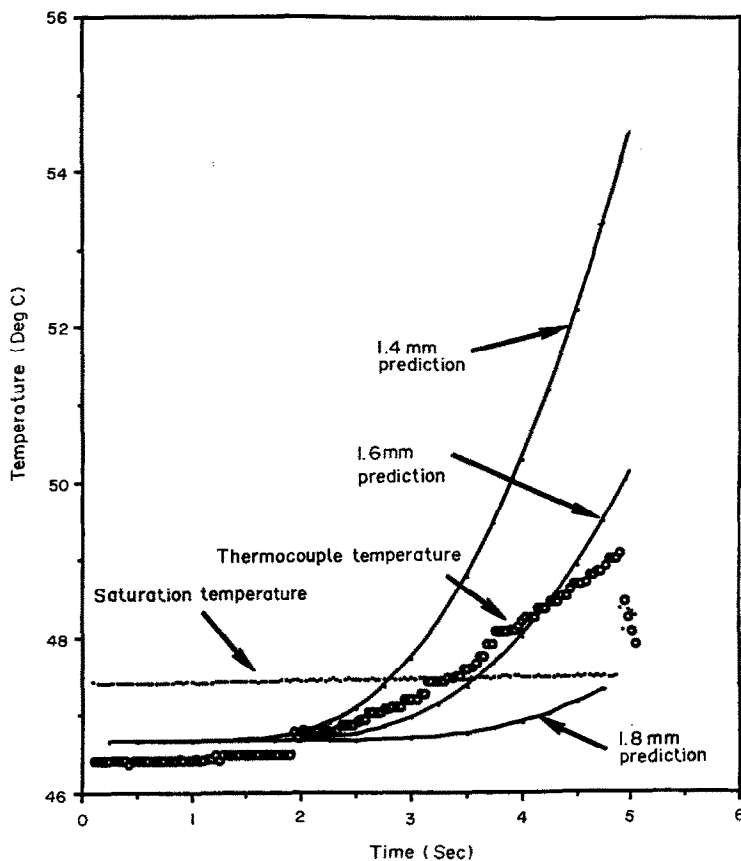
FIG. 5. Computed liquid temperature compared with measured thermocouple temperature.

dimensional transient temperature distribution within the liquid. Figure 5 shows the temperature rise measured by a thermocouple located at a nominal distance of 1.6 mm above the heater center. The uncertainty in the thermocouple location relative to the heater surface was ±0.2 mm, and the computed corresponding temperature variations are presented for the locations at 1.4, 1.6, and 1.8 mm above the heater surface, from equation (2). The measured thermocouple temperature variation is closest to the liquid temperature variations at 1.6 mm, the nominal location.

Measured transient heater surface temperatures such as presented in Fig. 4 assist in demonstrating the effects that the liquid temperature distributions, as influenced by buoyancy, have on the initial bubble dynamics. Photographs taken from high speed video and film frames will be used to illustrate such effects. A single view of the heating surface is inadequate for distinguishing bubble dynamic characteristics, since some of the vapor motion is obscured by other interface motion. In the current experiments, the boiling inception and the resulting bubble dynamics are observed from two orthogonal views: directly across and through the underside of the heater surface. Distinctly different types of early bubble motions, some previously not observed, are presented here and referred to as boiling spread or propagation, and may

be classified into six different categories. These will be described below and will include single or sequences of photographs of each. The first photograph of each sequence will list the experimental conditions of body force (a/g), heat flux input (q_T''), initial bulk liquid subcooling (ΔT_{sub}), the liquid saturation temperature (T_s) corresponding to the initial system pressure, and the initial bulk liquid temperature (T_i). The times in each figure refer to that from the onset of heating, and noteworthy features are indicated as appropriate. Within each of the categories below, one of two additional interesting types of behavior took place. (a) The formation of vapor bubble nuclei ahead of an advancing liquid–vapor front, which are at times pushed ahead by this front, and at other times absorbed into the front. (b) An advancing interface similar to that of 'normal' vapor bubble growth due to evaporation at the interface, regular at times and chaotic in other cases, but without the formation of the above vapor bubble nuclei ahead of the interface. The parameters under which these differences in behavior occur will be described, but their detailed origins are as yet unknown.

Categories of boiling propagation:
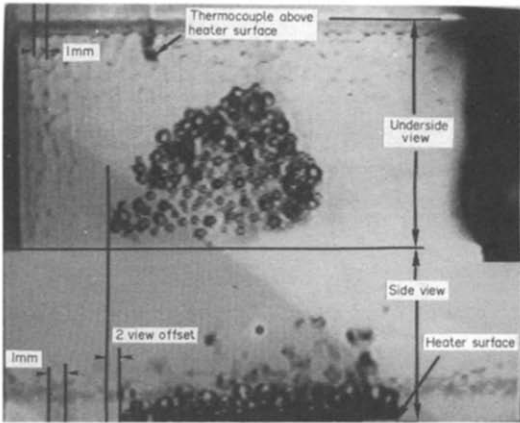
(A) advancement of interface by irregular protuberances;

FIG. 6. $a/g = +1$. Spreading of boiling by irregular protuberances. Time $= 1.306$ s; $q''_T = 7.68$ W cm^{-2}; $\Delta T_{sub} = 11.7°C$; $T_s = 60.4°C$; $T_i = 48.7°C$. Category (A).
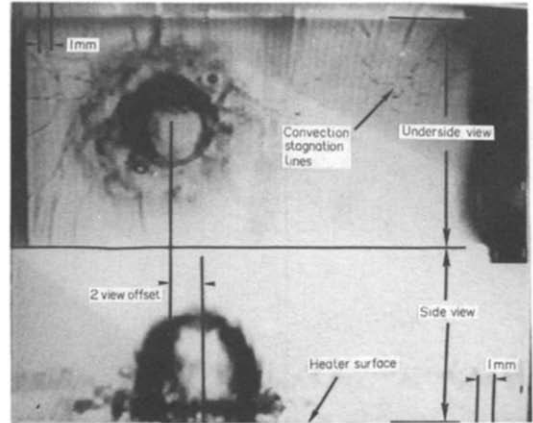

FIG. 7(a). $a/g = +1$. Early bubble formation and radial motion of thin vapor layer. Time $= 0.257$ s; $q''_T = 3.87$ W cm^{-2}; $\Delta T_{sub} = 11.4°C$; $T_s = 60.1°C$; $T_i = 48.7°C$. Category (B).

(B) growth of mushroom-like bubble with spreading along heater surface;

(C) orderly growth of bubble with a 'smooth' interface;

(D) orderly growth followed by onset of interface instabilities;

(E) energetic growth of bubble with unstable interface;

(F) slow motion of bubbles toward region of higher temperature.

(A) *Advancement of interface by irregular protuberances*

This category of boiling spread was observed only with the heating surface in the horizontal up position in earth gravity, and for the total power input to the gold film heating surface greater than 7 W cm^{-2}. For reference purposes, the critical heat flux for R113 in earth gravity is on the order of 15 W cm^{-2}. The vapor interface advances by irregular protuberances from bubbles, as shown in Fig. 6. The upper photo is through and from beneath the heating surface, and the lower portion presents the view across the heating surface. In Fig. 6 the boiling, which initiated at a single nucleating site, has spread over a large area of the heating surface in the presence of convection cells, some of which can still be seen. Bubbles depart from the heating surface due to buoyancy as the boiling propagates over the heating surface, and coalesce near the edge of the outwardly growing bubble front.

(B) *Growth of mushroom-like bubble with spreading along heater surface*

In contrast to the behavior in Fig. 6, if q''_T is reduced, in this case below 7 W cm^{-2}, then the considerably more dynamic events in Fig. 7(a) are typical. This category was observed only in earth gravity in the horizontal up orientation with q''_T less than 7 W cm^{-2}, and is presented in Figs. 7(a)–(c). Figure 7(a) shows

FIG. 7(b). Radial extension of thin vapor layer. Time = 0.282 s.
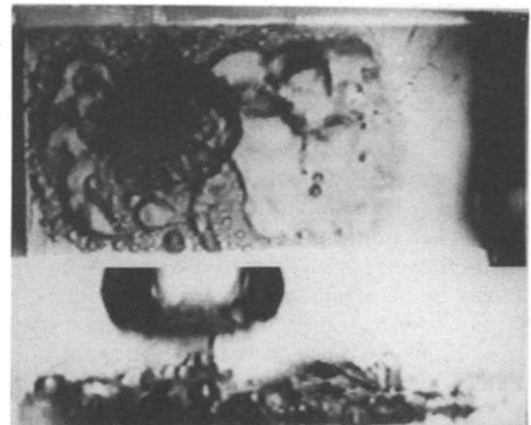

FIG. 7(c). Heater surface nearly covered by vapor layer and mushroom-shaped bubble departs from surface. Time = 0.289 s.

a mushroom shaped vapor bubble rising above the center of a thin vapor layer due to buoyancy, while the thin vapor layer itself advances outward. Convective stagnation lines are clearly visible in the upper portion

of the photo of Fig. 7(a), while the thin vapor layer surrounding the large growing bubble is observed to move radially outward in Figs. 7(a) and (b). The side views show that small vapor bubbles form on the surface of this thin vapor layer. The vapor has covered most of the heating surface in Fig. 7(c), and in the view across the heating surface, the large bubble is dynamically departing with a time interval of only 7 milliseconds between Figs. 7(b) and 7(c). The upward bubble motion entrains liquid and causes more disturbances over the outward growing vapor layer.

Okuyama et al. [7] observed a similar type of bubble growth with a horizontal up heater orientation in earth gravity, also using a step in heat flux (q_i'' on the order of 20 to 40 W cm^{-2}) applied to a 7 micron thick copper foil (0.4 cm wide by 4 cm long) laminated to an epoxy plate, and also with R113 at variable pressures less than 500 kPa. In the present study, by contrast, the heat flux to the liquid is considerably smaller, with the largest q_i'' on the order of 1.4 W cm^{-2}, and the pressure was on the order of 120 kPa.

(C) Orderly growth of bubble with a 'smooth' interface

This was observed only in earth gravity with the heating surface in the horizontal down orientation, so that the upward buoyancy force held the vapor bubble against the heating surface, producing a pancake-like bubble with a 'smooth' interface, as shown in Fig. 8. The initial bubble grew outward in an orderly manner from one location near the edge of the heating surface. This bubble eventually moved away from the location at which it first originated, and a second bubble formed at this location and coalesced with the first one, resulting in the bubble seen in both views of Fig. 8. The approximate bubble radius varied with the square root of time. After the bubble had grown past the edges of the gold film heater, condensation occurred at some peripheral locations and the liquid then re-wetted the heater.
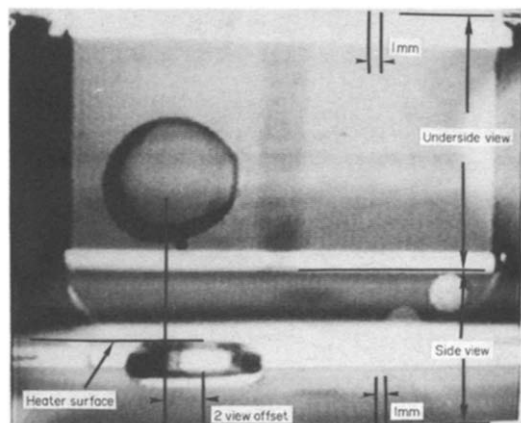

FIG. 8. $a/g = -1$. Pancake-like bubble with a 'smooth' interface. Time $= 0.419$ s; $q_T'' = 7.18$ W cm^{-2}; $\Delta T_{sub} = 2.2°C$; $T_s = 51.9°C$; $T_i = 49.7°C$. Category (C).

(D) Orderly growth followed by onset of interface instabilities

This consists of an initially orderly growth of either a hemispherical bubble, in the case of microgravity, or a pancake-like one for the heater surface in earth gravity in the horizontal down position, which then gives way to dynamic growth. The lower heat flux, higher subcooling, and longer time to boiling incipience given in Fig. 9(a) are in contrast to the experiment of Fig. 8, where the heater surface is also horizontal down in earth gravity. The bubble interface with this behavior was initially smooth and then developed disturbances, appearing to rupture either on the surface or at the base of the bubble, initiating the onset of the dynamic growth. Figs. 9(a)–(c) show the history of the boiling spread associated with the apparent rupturing of the bubble occurring at the periphery of the bubble base. Figure 9(a) shows the bubble with a disturbance, which advances radially outward at the heater surface and appears one frame after the onset of boiling. In Fig. 9(b), 12 milliseconds later, the bubble interface has disturbances in the form
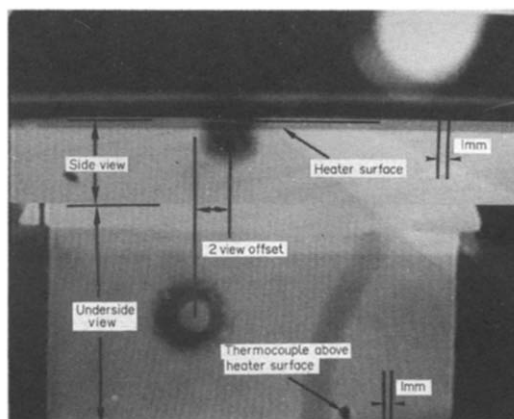

FIG. 9(a). $a/g = -1$. Orderly growth followed by onset of interface disturbances at bubble periphery. Time $= 10.214$ s; $q_T'' = 3.57$ W cm^{-2}; $\Delta T_{sub} = 11.3°C$; $T_s = 60.4°C$; $T_i = 49.2°C$. Category (D).
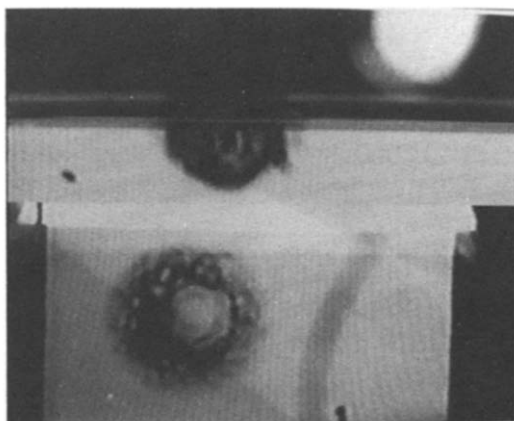

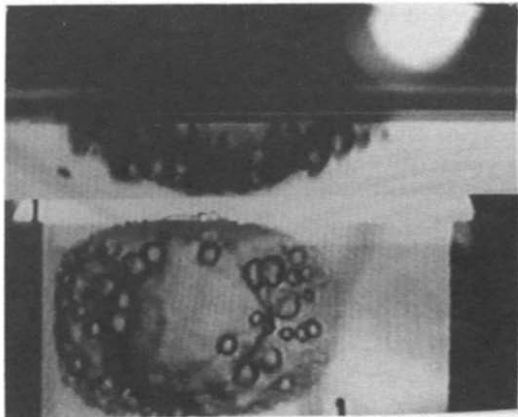FIG. 9(b). Large-scale interface bubbles. Time $= 10.226$ s.

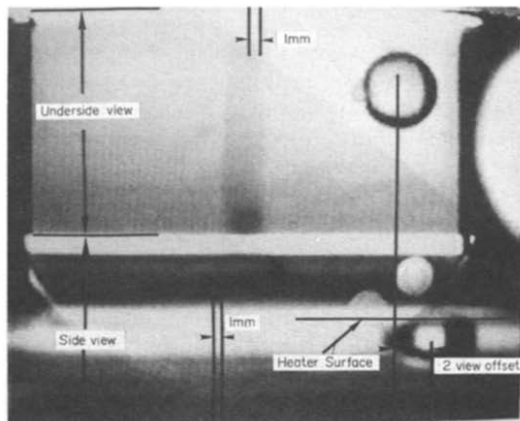FIG. 9(c). Heater surface nearly covered by vapor, interface with remaining satellite bubbles. Time = 10.238 s.

FIG. 10(a). $a/g = -1$. Onset of interface disturbance on bubble periphery. Time = 28.890 s; $q''_T = 1.93$ W cm^{-2}; $\Delta T_{sub} = 2.3°C$; $T_s = 52.0°C$; $T_i = 49.7°C$. Category (D).

of new vapor bubbles, but no thin vapor layer as in Figs. 7(a). This motion was accompanied by a spike increase in the system pressure. Fig. 9(c) provides a clear view of these interface bubbles.

Another type of boiling spread associated with the appearance of rupturing of a smooth and symmetrical bubble surface is illustrated in Figs. 10(a)–(c). The breaking of the liquid–vapor interface in Fig. 10(c) occurs on the bubble periphery near the warmest part of the heater, the heater center. Figures 10(b) and (c) show smaller bubbles on the outwardly moving interface of the larger bubble. Category (D) phase change dynamics described here were observed to occur either in microgravity or in earth gravity with the heater surface in the horizontal down position, and are generally associated with low heat flux levels and longer heating periods prior to the onset of boiling. The heat flux resulting in the category (C) boiling spread of Fig. 8, with a smooth interface, was greater than that here with all conditions otherwise the same.

(E) *Energetic growth of bubble with unstable interface*

This category is referred to as energetic boiling propagation, and characterized by the appearance of initially uniform small scale protuberances over the entire liquid vapor interface. The sequence of photos in Figs. 11(a)–(g) are from an experiment in microgravity and illustrate the phase change dynamics associated with this kind of boiling propagation, and is reproducible for similar conditions. In the upper portion of Fig. 11(a), the conduction thermal boundary layer is visible as a line parallel to and slightly above the heater surface. A shadow is marked in the photo, indicating the nucleation location and extent. Figure 11(b) shows the onset of boiling at seven locations in the view from beneath the heating surface, and a large vapor mass above the thermal boundary layer in the view across the heater surface, corresponding to the location of the shadow referred to above. Small scale protuberances are visible, but are
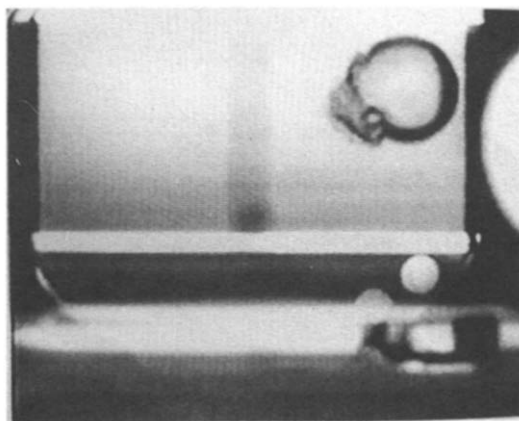

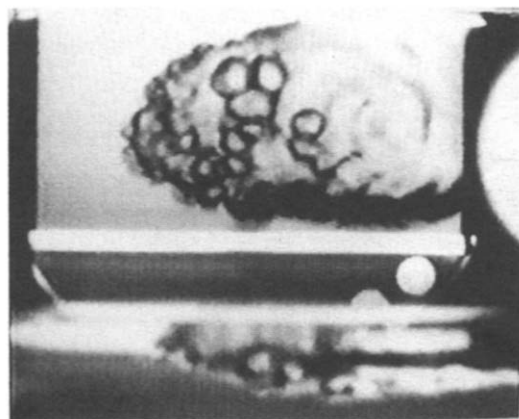FIG. 10(b). Onset of dynamic vapor growth. Time = 28.898 s.

FIG. 10(c). Vapor with interface bubbles nearly covers heater surface. Time = 28.898 s.

somewhat blurred because of the high initial growth rate. The protuberances are more distinguishable five milliseconds later in Fig. 11(c), and are still identifiable in Figs. 11(d) and (e), although they have grown to larger sizes. Figure 11(f) shows that the
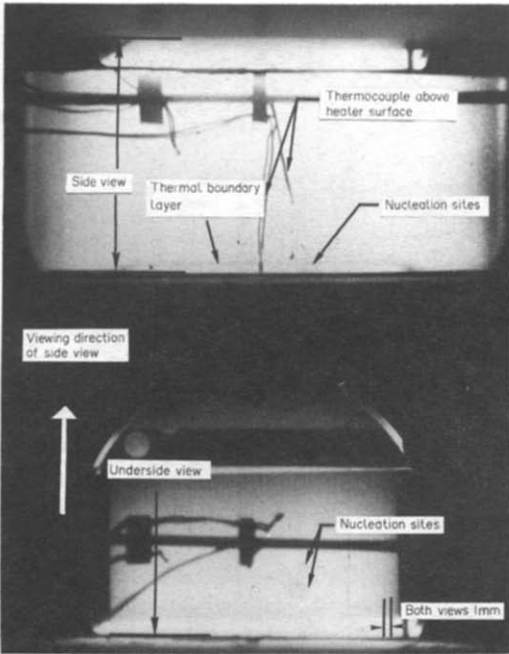
FIG. 11(a). Microgravity. Boiling inception near saturation conditions with thermal boundary layer visible. Time = 4.810 s; $q_T'' = 5.40$ W cm^{-2}; $\Delta T_{sub} = 0.4°C$; $T_s = 47.2°C$; $T_i = 46.8°C$. Category (E).
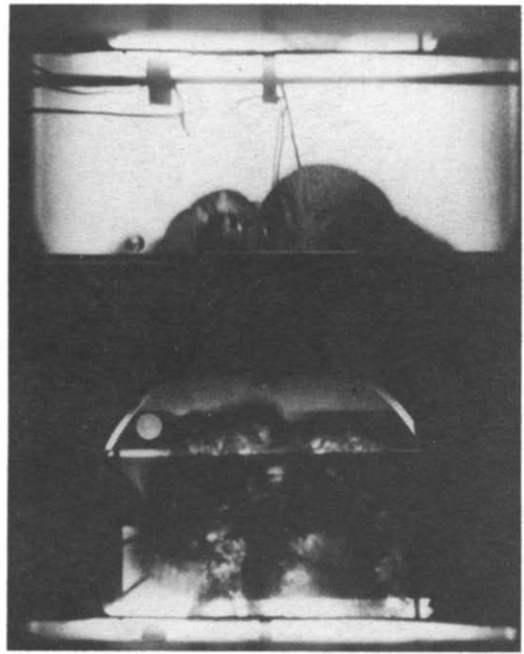

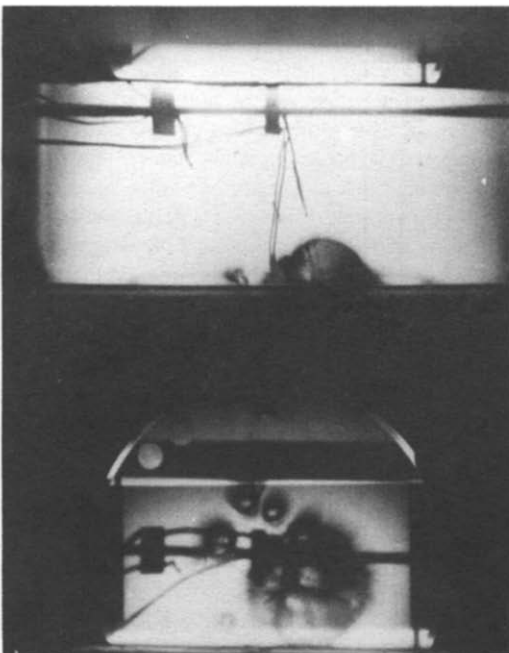FIG. 11(c). Vapor nearly covers entire heater surface. Time = 4.818 s.

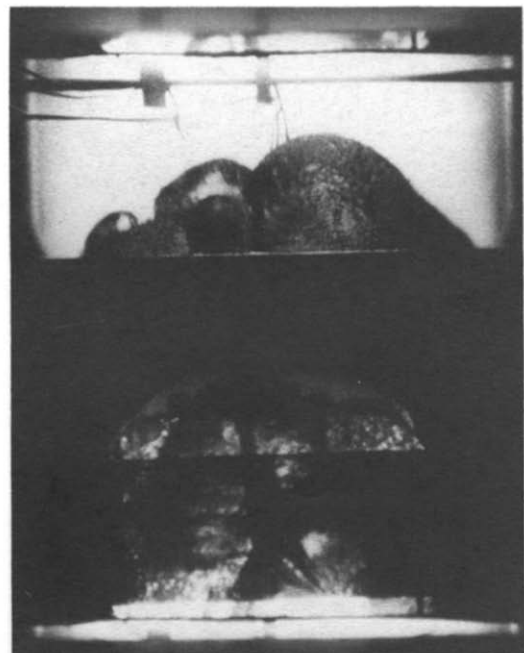FIG. 11(b). Energetic, rapid bubble growth. Time = 4.813 s.

FIG. 11(d). Small scale protuberances are more distinguishable. Time = 4.820 s.
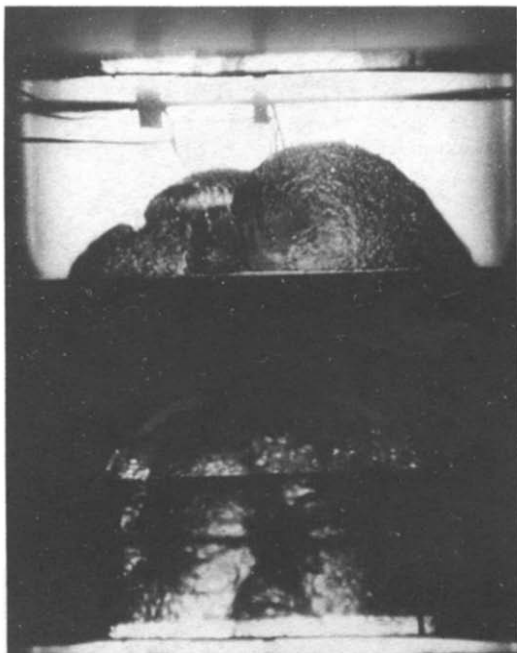
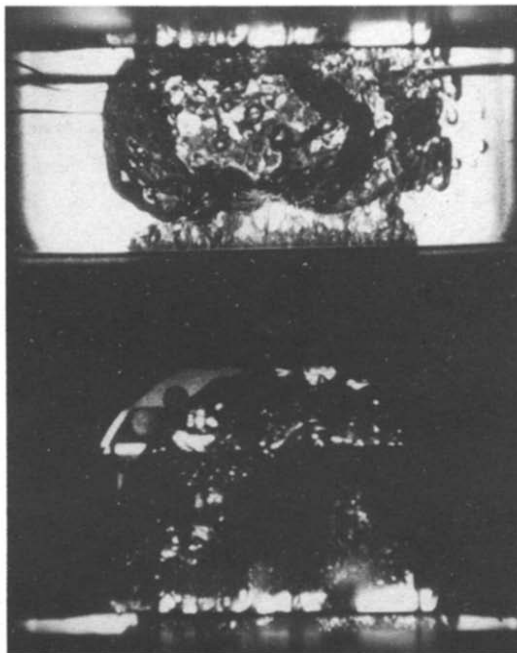FIG. 11(e). Dynamic growth continues. Time = 4.840 s.

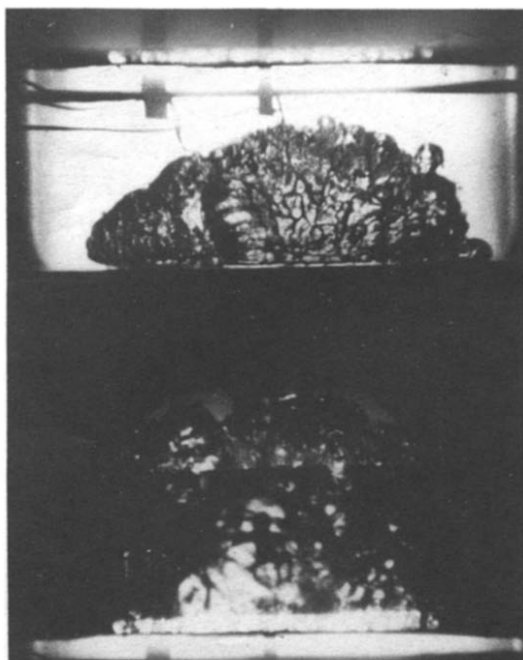FIG. 11(g). Bulk liquid momentum lifts vapor off heating surface. Time = 4.973 s.

FIG. 11(f). Protuberances have grown. Time = 4.890 s.

The type of interfacial form and motion shown in Figs. 11(a)–(g) has not been previously observed to the knowledge of the authors. It is believed that the small scale protuberances, which are the result of local pressure disturbances possibly arising from the combination of surface tension and local temperature gradients, greatly increase the liquid–vapor interface surface area, which then results in a very large evaporation rate. The pressure disturbances resulting from this large mass flux create more protuberances which drive the unstable growth of the vapor mass across the heating surface. This type of boiling spread was observed only in microgravity with minimum subcooling. The lower limit of heat flux that might produce this could not be established at this time because the time of five seconds presently available in microgravity was too short for boiling incipience to take place. In the drop tower tests, a q_T'' of 4 W cm^{-2} was the lower limit.

Small scale interface disturbances and large growth rates have been observed by Sturtevant and Shepherd [8] and with similar conditions by McCann *et al.* [9], but involved the superheating of liquid drops rather than the case of a bulk liquid here. In ref. [8], a droplet of butane immersed in immiscible ethylene glycol in a bubble column apparatus at the homogeneous nucleation temperature vaporized explosively. Wrinkles were observed at the periphery of the bubble similar to those shown in Figs. 11(a)–(e), and were speculated to be the result of the so-called Landau mechanism of instability, described in ref. [10]. Sturtevant and Shepherd used pressure measurements to estimate the evaporation rate associated with the

vapor has coalesced into a single large mass, some small bubbles have separated from this vapor mass, and the protuberances are larger. The rapidly growing vapor was accompanied with a momentary spike in the pressure. The rapid evaporation imparts momentum to the liquid bulk, which then lifts the vapor off the heating surface, as in Fig. 11(g). The early growth rate of the vapor interface is on the order of 4 m s^{-1}.

observed instability, and found that the evaporation rate was two orders of magnitude greater than that predicted by conventional bubble-growth theories. They believed that the large evaporation rate at the wrinkled liquid–vapor interface generated vorticity responsible for the Landau instability. Vapor bubble growth in slightly superheated liquids has been investigated extensively, but such wrinkling of the interface was not observed.

The present experiments which result in the category (E) spreading defined here are different from those of ref. [8] in that the liquid was heated from a solid boundary, and the heater surface temperature was below the homogeneous nucleation temperature for the given liquid pressure, with $T_w/T_{hom} = 0.9$ at nucleation. The heater surface superheat at incipient boiling here was nominally 75°C, and is large when compared to other values observed for R113 on glass in earth gravity, as described in You *et al.* [11].

(F) *Slow motion of bubbles toward region of higher temperature*

This type of boiling spread involved orderly and slow bubble growth and was observed for microgravity and for the inverted heater surface in earth gravity. q''_T was relatively large, greater than 7.2 W cm^{-2} for these instances. The propagation consisted of small bubbles forming and then moving toward the center of the thin film heater, the warmest part, and coalescing there, as shown in Figs. 12(a)–(d). The first bubble appeared at the edge of the heater and subsequently moved toward the center, with more
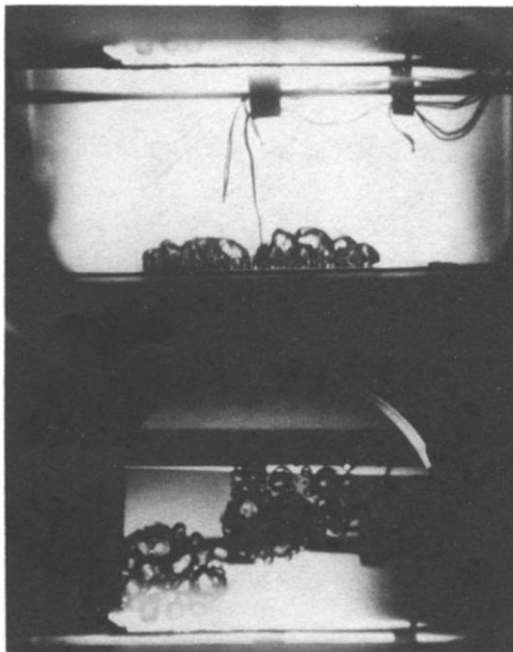

FIG. 12(b). More bubbles nucleate and grow toward heater center. Time = 0.920 s.
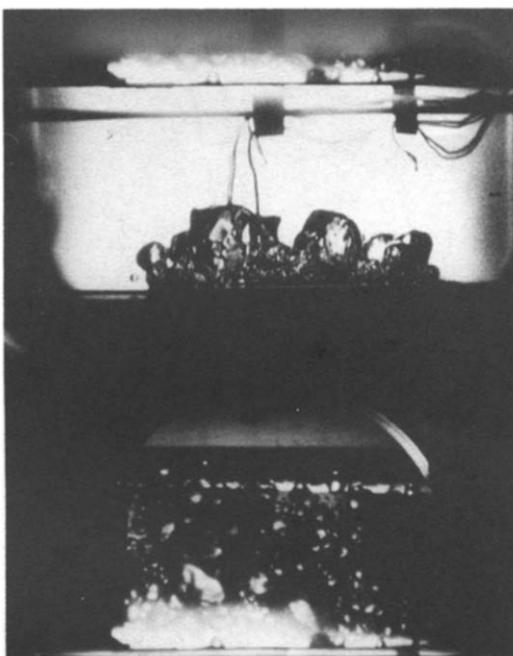

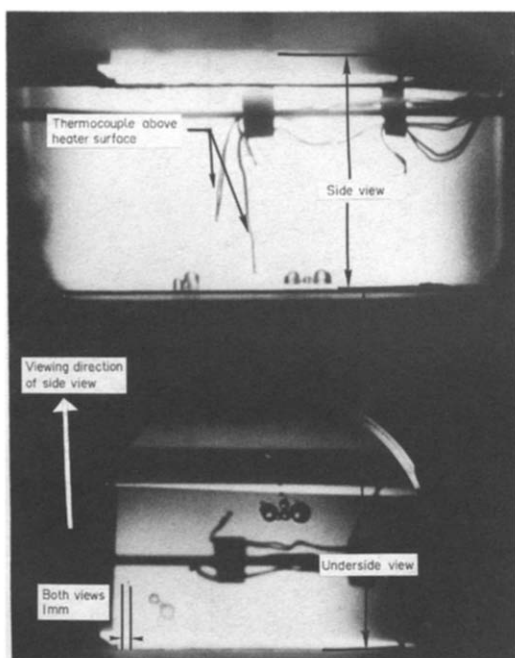FIG. 12(c). Bubbles cover heater surface and coalesce. Time = 1.230 s.

FIG. 12(a). Microgravity. Bubbles nucleating and growing from two sites. Time = 0.718 s; $q''_T = 7.80$ W cm^{-2}; $\Delta T_{sub} = 11.1$°C; $T_s = 58.6$°C; $T_i = 47.5$°C. Category (F).

bubbles forming at the original incipient boiling location. Another location on the left side of the heater surface later became active as a boiling site, as seen in Fig. 12(a). Additional bubbles have emanated from the two nucleation sites in Fig. 12(b), and meet near the heater center, where they grow and coalesce as in Fig. 12(c), forming one large bubble surrounded by
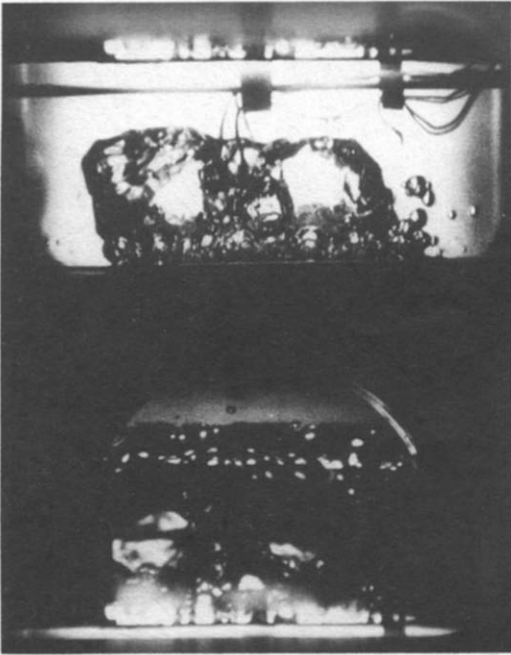
FIG. 12(d). Large vapor bubble with smaller bubbles at periphery. Time = 4.762 s.

bubbles generated at the heater edges, as seen in Fig. 12(d). As can be seen, some vapor bubbles have separated and formed individual bubbles in the bulk liquid as a result of the interface dynamics taking place.

DISCUSSION

For experiments conducted in microgravity, the liquid superheat temperature distribution at the moment of boiling inception can be computed by the conduction analysis described earlier, and is demonstrated in Fig. 13. Temperature distributions which result in boiling spread categories (A), (B), and (C) cannot be given in a plot such as Fig. 13 since these categories were observed only in earth gravity, where natural convection was present. Measured heater surface superheat temperatures are included in Fig. 13, and the coincidence with the computed heater surface temperatures confirm the accuracy of the calculated liquid superheat temperature distributions.

Results shown are for different levels of heat flux and three levels of subcooling. The largest calculated superheated thermal boundary layer thickness at
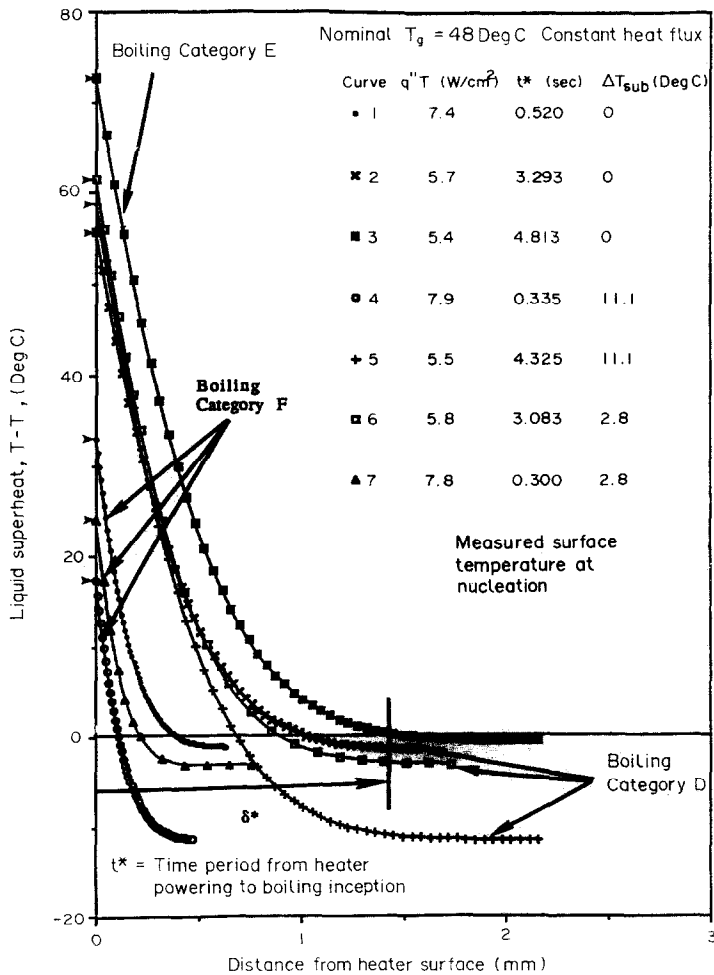

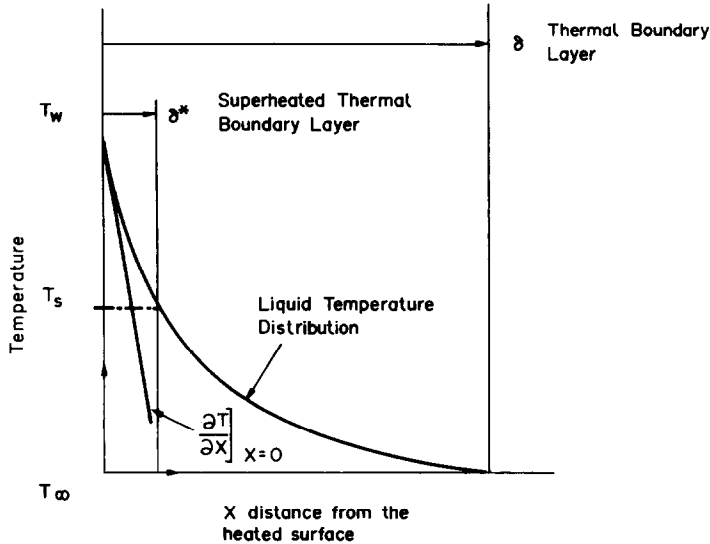FIG. 13. Computed liquid superheat at boiling inception in microgravity.

Fig. 14. Concepts of superheated thermal boundary layer and thermal boundary layer.

incipient boiling, δ^*, is denoted for illustrative purposes in addition to the computed liquid temperature distributions at the time of boiling inception. δ, the thermal boundary layer, is always greater than δ^*. Both the thermal boundary layer, δ, and the superheated thermal boundary layer, δ^*, are shown for illustrative purposes in Fig. 14. Boiling spread categories (D) and (E) are associated with larger values of δ^* than that corresponding to category (F).

The type of boiling spread observed is related to the amount of thermal energy in the superheated thermal boundary layer, and superheated thermal boundary layers with more energy can be expected to exhibit more dynamic boiling propagation than those with less energy. The change in internal energy of the superheated thermal boundary layer per heater surface area up to the point of boiling inception is a function of both the imposed heat flux and the total time to the inception of boiling, and can be estimated by

$$\Delta U^* = \rho c \int_0^{\delta^*(t)} (T(x) - T_s)\, dx. \qquad (3)$$

This is represented in Fig. 13 by the area between the superheat temperature curve and the horizontal axis. A relatively small increase in internal energy of the superheated thermal boundary layer is associated with the category (F) spreading, while the boiling spread with a relatively large increase in energy of the superheated thermal boundary layer are of the category (D) type. On occasions with very large increases in the energy of the superheated thermal boundary layer, category (E) type boiling spread results.

CONCLUSIONS

Known temperature distributions in the heated liquid at the moment of boiling incipience, obtained

in microgravity, were shown to characterize the subsequent boiling propagation taking place across the heated surface. Large superheated thermal boundary layers formed in the conditions of microgravity and low heat flux levels on a 'smooth' heater surface are associated with a particularly energetic type of boiling spread previously unobserved, which is believed to be the result of an interfacial instability driven by a large mass flux across the wrinkled liquid–vapor interface.

Buoyancy was shown to greatly affect the phase change dynamics associated with incipient boiling. In producing fluid motion, the liquid temperature distribution is affected during heating, as is the subsequent boiling propagation. Certain types of boiling spread, such as the energetic type of spreading, were observed only in microgravity, and not in earth gravity for either the horizontal up or the horizontal down heater surface orientations. Buoyancy induced convective motion reduces the energy of the superheated thermal boundary layer that would otherwise be available for such energetic boiling propagation. Buoyancy carried vapor bubbles away from the heater surface when the heater surface was in the horizontal up orientation in earth gravity, but held vapor bubbles at the heater surface for the horiontal down orientation.

REFERENCES

1. M. Ulucakli, Nucleate pool boiling with increased acceleration and subcooling, Ph.D. Thesis, University of Michigan, Ann Arbor (1987).
2. E. Oker and H. Merte, A study of transient effects leading up to inception of nucleate boiling, Proc. 6th Int. Heat Transfer Conf., Toronto, August 1978, 139–144 (1978).

3. L. X. Ngheim, Holographische Untersuchung Des Instationaren Siedens, Ph.D. Thesis, Munich (1980).
4. E. Oker and H. Merte, Transient boiling heat transfer in saturated liquid nitrogen and F113 at standard and zero gravity, University of Michigan NASA Report No. 074610-52-F (1973).
5. J. Straub, M. Zell and B. Vogel, Pool boiling in a reduced gravity field, presented at the Int. Heat Transfer Conf., Jerusalem, Israel (1990).
6. J. S. Ervin, Incipient boiling in microgravity, Ph.D. Thesis, University of Michigan, Ann Arbor (1991).
7. K. Okuyama, Y. Kozawa, A. Inoue and S. Aoki, Transient boiling heat transfer characteristics of R113 at large

8. stepwise power generation, Int. J. Heat Mass Transfer 31, 2161-2174 (1988).
9. B. Sturtevant and J. Shepherd, Evaporative instability at the superheat limit, Appl. Sci. Res. 38, 85-97 (1982).
9. H. McCann, L. Clarke and A. Masters, An experimental study of vapor growth at the superheat limit temperature, Int. J. Heat Mass Transfer 32, 1077-1093 (1989).
10. L. Landau, On the theory of slow combustion, Acta Phys.-chim. URSS 19, 77-85 (1944).
11. S. M. You, T. W. Simon, A. Bar-Cohen and W. Tong, Experimental investigation of nucleate boiling incipience with a highly wetting dielectric fluid (R-113), Int. J. Heat Mass Transfer 33, 105-117 (1990).

EBULLITION VARIABLE EN RESERVOIR AVEC MICROGRAVITE

Résumé—Des expériences d'ébullition nucléée variable en réservoir de R 113 sont conduites pendant des temps courts de microgravité et de gravité terrestre, avec différentes orientations de surface chauffée et plusieurs sous-refroidissements. La surface de chauffage est un film transparent d'or déposé sur un substrat en quartz, ce qui permet en même temps les mesures de température de surface et la visualisation du mécanisme d'ébullition par dessous. Pour les expériences de microgravité avec une température initiale uniforme et aucun mouvement de fluide, la distribution de température dans le R 113 au moment du départ de l'ébullition est connue. Des caméras à grande vitesse avec vues à travers la surface chauffée enregistrent l'expression de l'ébullition à la surface du chauffoir et on fait un classement en six (6) catégories distinctes.

BEHÄLTERSIEDEN IM ÜBERGANGSBEREICH BEI MIKROGRAVITATION

Zusammenfassung—Das Behältersieden im Übergangsbereich wird mit R113 bei Mikrogravitation und Erdgravitation untersucht. Dabei wird die Orientierung der Heizfläche und die Unterkühlung variiert. Die Heizfläche besteht aus einem durchsichtigen Goldfilm, der auf einem Quarzglasträger aufgesputtert wurde. Er ermöglicht die Messung der Heizflächentemperatur und erlaubt die Beobachtung des Siedevorgangs von der Unterseite. Für die Versuche bei Mikrogravitation ist die Temperaturverteilung in R113 bei Siedebeginn bekannt, da die anfänglichen Temperaturen einheitlich waren und keine Fluidbewegung stattfand. Hochgeschwindigkeitskameras mit paralleler und senkrechter Blickrichtung zur Heizfläche zeichnen die Ausbreitung des Siedevorgangs an der Heizfläche auf. Sie läßt sich in 6 Gruppen einteilen.

НЕСТАЦИОНАРНОЕ КИПЕНИЕ В БОЛЬШОМ ОБЪЕМЕ ПРИ МИКРОГРАВИТАЦИИ

Аннотация—Проведены нестационарные эксперименты по пузырьковому кипению фреона 113 в большом объеме при небольших временах воздействия микрогравитации и земной гравитации, различных ориентациях поверхности нагревателя и значениях недогрева. Поверхностью нагрева служит прозрачная пленка из золота, нанесенная на кварцевую подложку, которая одновременно позволяет проводить измерения температуры поверхности и наблюдения снизу за процессом кипения. В экспериментах по микрогравитации, в которых начальная температура однородна и отсутствует движение жидкости, распределение температуры во фреоне 113 в момент начала кипения известно. С помощью высокоскоростной киносъемки регистрируется распространение кипения поперек поверхности нагревателя, которое подразделяется на шесть четких стадий.